Phys. Lett. B 868 (2025) 139811

Contents lists available at ScienceDirect

Physics Letters B

journal homepage: www.elsevier.com/locate/physletb

Letter

Lattice QCD study of the $\chi_{c1} \to J/\psi\,\gamma$ decay

Damir Bečirević [a], Roberto Di Palma [b], Roberto Frezzotti [c], Giuseppe Gagliardi [b,*], Vittorio Lubicz [b], Francesco Sanfilippo [d], Nazario Tantalo [c]

[a] IJCLab, Pôle Théorie (Bat. 210), CNRS/IN2P3 et Université Paris-Saclay, 91405, Orsay, France
[b] Dipartimento di Matematica e Fisica, Università Roma Tre and INFN, Sezione di Roma Tre, Via della Vasca Navale 84, I-00146, Rome, Italy
[c] Dipartimento di Fisica and INFN, Università di Roma "Tor Vergata", Via della Ricerca Scientifica 1, I-00133, Roma, Italy
[d] Istituto Nazionale di Fisica Nucleare, Sezione di Roma Tre, Via della Vasca Navale 84, I-00146, Rome, Italy

ARTICLE INFO

Editor: Dr Francois Gelis

Keywords:
Lattice QCD
Radiative charmonia decays

ABSTRACT

We present the results of our lattice QCD computation of the electric (E_1) and magnetic (M_2) form factors relevant to the $\chi_{c1} \to J/\psi\,\gamma$ decay by using the gauge field configurations produced by the Extended Twisted Mass Collaboration with $N_f = 2+1+1$ dynamical Wilson-Clover twisted mass fermions at four different lattice spacings with physical dynamical u, d, s and c quark masses (except for the coarsest lattice for which the lightest sea quark corresponds to a pion with $m_\pi \simeq 175$ MeV). In the continuum limit, we obtain $\Gamma(\chi_{c1} \to J/\psi\,\gamma) = 0.3265(79)$ MeV, which agrees to $(1 \div 2)\sigma$ with the experimental results and disagrees with a previous (unquenched) lattice QCD calculation. Our result for the magnetic quadrupole fractional transition amplitude, $a_2 = M_2/\sqrt{E_1^2 + M_2^2} = -0.0666(22)$, is in agreement with the experiment and represents an improvement by a factor of about 30 with respect to the only existing (quenched) lattice QCD result.

1. Introduction

In recent years, the radiative decays of heavy quarkonia have attracted considerable phenomenological interest. The study of the so called electric dipole (E1) and magnetic dipole (M1) transitions, such as $h_{c(b)} \to \eta_{c(b)}\gamma$, $J/\psi \to \eta_c\gamma$ and $\Upsilon \to \eta_b\gamma$, can give further insight in the internal structure and dynamics of heavy quarkonium states, conveniently described by an appropriate effective field theory [1–4]. Further motivation for studying these decay modes arises from the searches of a light (flavorless) pseudoscalar state, originating from beyond the Standard Model (BSM), that could either be a candidate for dark matter or act as a portal that mediates interaction between the Standard Model (SM) fermions and the dark matter constituents. In that respect the modes with $\eta_{c,b}$ in the final state are particularly interesting, as the observed state could be a mixture of the genuine $\eta_{c,b}$ (SM) and the light BSM pseudoscalar boson. To disentangle such a mixing, it is essential to keep the SM amplitude under theoretical control, which is where lattice QCD provides a key contribution. In that context we recently investigated the $1^{+-} \to 0^{-+} + \gamma$ decay, both in the case of charmonia and bottomonia, which allowed us to predict for the first time the full width of the h_b meson, $\Gamma(h_b) = (88 \pm 13)$ keV, and to improve $\Gamma(h_c \to \eta_c\gamma)$ by more than a factor of two with respect to the previous lattice calculations.[1]

In this paper, instead, we focus on the $1^{++} \to 1^{--}\gamma$ channel; the $\chi_{c1} \to J/\psi\,\gamma$ decay mode. That channel is interesting because it has been studied experimentally in great detail so that a comparison between theory (lattice QCD) and experiment, without involving weak interaction, can provide a fine verification of the validity of the precision lattice QCD computation of hadronic quantities. Regarding experiment, the decay width of this channel has been measured by the Fermilab collaborations [5,6] and the current average is $\mathcal{B}(\chi_{c1} \to J/\psi\,\gamma) = (34.3 \pm 1.3)\%$ [7]. The charm factories at CLEO [8] and BES-III [9] went a step beyond and made an accurate angular analysis of decays of the χ_{cJ} resonances, which then allowed them to extract the so called magnetic quadrupole fractional amplitude,

$$a_2 = \frac{M_2}{\sqrt{E_1^2 + M_2^2}}\,, \tag{1}$$

[1] We use the standard spectroscopic notation to label the states, J^{PC}, where J stands for the quantum number associated to the angular momentum (spin), while P and C correspond to state's parity and charge conjugation, respectively.

* Corresponding author.
E-mail addresses: damir.becirevic@ijclab.in2p3.fr (D. Bečirević), roberto.dipalma@uniroma3.it (R. Di Palma), frezzotti@roma2.infn.it (R. Frezzotti), giuseppe.gagliardi@roma3.infn.it (G. Gagliardi), vittorio.lubicz@roma3.infn.it (V. Lubicz), francesco.sanfilippo@infn.it (F. Sanfilippo), nazario.tantalo@roma2.infn.it (N. Tantalo).

https://doi.org/10.1016/j.physletb.2025.139811
Received 4 July 2025; Accepted 6 August 2025
Available online 8 August 2025

where $E_1 \equiv E_1(0)$ and $M_2 \equiv M_2(0)$ are respectively the electric and magnetic form factors describing $\chi_{c1} \to J/\psi\,\gamma$ (see Eq. (3) below). The results obtained by CLEO and BES-III, $a_2^{\rm CLEO} = -0.0626(67)$ and $a_2^{\rm BES-III} = -0.0740(47)$, have an accuracy of $O(10\,\%)$ and $O(6\,\%)$, and differ from each other by 1.4σ.

Concerning the previous lattice QCD studies, this mode has been elaborated for the first time in Refs. [10,11] where the computation of the relevant form factors has been performed on a single (anisotropic) lattice in the quenched approximation. Note that they computed the form factors $E_1(q^2)$ and $M_2(q^2)$ at $q^2 \neq 0$, and then extrapolated them to E_1 and M_2, corresponding to the on-shell photon ($q^2 = 0$). For that reason they could not provide a reliable determination of a_2. Instead, for the decay rate, which is dominated by the electric form factor $E_1(0)$, they reported $\Gamma(\chi_c \to J/\psi\,\gamma) = 0.27(7)$ MeV. To date the only unquenched result for this decay has been reported in Ref. [12], obtained by using the gauge field configurations with $N_f = 2$ twisted mass quarks at two lattice spacings. The decay rate was estimated to be $\Gamma(\chi_{c1} \to J/\psi\,\gamma) = (73 \pm 20)$ keV, thus much smaller than both the result of Ref. [11], and the experiment $\Gamma(\chi_{c1} \to J/\psi\,\gamma)^{\rm exp} = 0.288(18)$ MeV [7].

In this work we seek to improve on the lattice results by performing a high precision calculation of both E_1 and M_2 form factors. In so doing we employ four different lattice spacings in the range $a \in [0.058 - 0.09]$ fm. A particularly subtle point, when dealing with twisted mass quarks, is to choose an appropriate interpolating operator for the χ_{c1} state, i.e. the one that avoids mixing of the desired $J^{PC} = 1^{++}$ with unwanted $J^{PC} = 1^{--}$ and/or $J^{PC} = 1^{+-}$ states, which are lighter and thus would obstruct the overlap with χ_{c1}. Such a mixing is due to the parity breaking in the twisted mass QCD formulation and therefore it can show up even at zero three-momentum. We will show that this problem can be solved, and then through a high-statistics computation of the relevant two- and three-point correlation functions we determine both the electric and magnetic form factors with $O(1-3\,\%)$ accuracy. We anticipate our final results, namely

$$\Gamma(\chi_{c1} \to J/\psi\,\gamma) = 0.3265(79)\ \text{MeV},\ a_2 = -0.0666(22). \tag{2}$$

The remainder of this paper is organized as follows. In Section 2 we discuss the lattice setup employed for the determination of the two relevant form factors, focusing in particular on the choice of the interpolating operators adopted to isolate the χ_{c1} and the J/ψ. In Section 3 we present the results of our analysis of the J/ψ and χ_{c1} masses, as well as the results for the two form factors E_1 and M_2, including the discussion of all systematic effects including those associated with the correct isolation of the initial and final hadronic states and with the continuum-limit extrapolation. Finally, in Section 4, we compare our results with experimental measurements and existing theoretical calculations, and in Section 5 we present our conclusions and discuss directions for future improvements.

2. $\chi_{c1} \to J/\psi$ Form factors and lattice setup

We adopt the following decomposition of the transition matrix element describing the decay $\chi_{c1} \to J/\psi\gamma^*$ [10]:

$$\begin{aligned}
&\langle J/\psi(k,\varepsilon)|J^\mu_{\rm em}|\chi_{c1}(p,\eta)\rangle \\
&\quad = \frac{iQ_c}{4\sqrt{2}\,\Omega(q^2)}\epsilon^{\mu\nu\rho\sigma}(p-k)_\sigma \times \Bigg\{ 2\big[E_1(q^2)+M_2(q^2)\big](\eta^*\cdot k)\,\varepsilon_\nu(p+k)_\rho \\
&\quad + 2\frac{m_{J/\psi}}{m_{\chi_{c1}}}\big[E_1(q^2)-M_2(q^2)\big](\varepsilon\cdot p)\eta^*_\nu(p+k)_\rho \\
&\quad + \frac{C_1(q^2)}{\sqrt{q^2}}\Bigg[-4\Omega(q^2)\,\eta^*_\nu\varepsilon_\rho + \Bigg[\Big(m^2_{\chi_{c1}} - m^2_{J/\psi} + q^2\Big) \\
&\quad (\eta^*\cdot k)\,\varepsilon_\nu + \Big(m^2_{\chi_{c1}} - m^2_{J/\psi} - q^2\Big)(\varepsilon\cdot p)\,\eta^*_\nu\Bigg](p+k)_\rho\Bigg]\Bigg\},
\end{aligned} \tag{3}$$

where $J^\mu_{\rm em}$ is the electromagnetic current,

$$J^\mu_{\rm em}(x) = \sum_{f=u,d,s,c} J^\mu_f(x) = \sum_{f=u,d,s,c} Q_f\,\bar q_f(x)\gamma^\mu q_f(x), \tag{4}$$

with the sum running over all quark flavors, $q_f(x)$ being the quark field, and Q_f its electric charge in units of $e = \sqrt{4\pi\alpha_{\rm em}}$. In Eq. (3), p and k are the momenta of χ_{c_1} and J/ψ respectively, while η and ε are their respective polarization vectors. Finally, $E_1(q^2)$, $M_2(q^2)$ and $C_1(q^2)$ are the form factors, functions of $q^2 = (p-k)^2$, while the kinematic function $\Omega(q^2) = (p\cdot k)^2 - m^2_{J/\psi} m^2_{\chi_{c1}}$. The form factor $C_1 \equiv C_1(0)$ does not contribute to the matrix element of the physical $\chi_{c1} \to J/\psi\gamma$ and will not be discussed in the following. Note also that we slightly modified the decomposition of Refs. [10–12] in order to make both E_1 and M_2 dimensionless. The decay rate then reads:

$$\Gamma\big(\chi_{c1} \to J/\psi\gamma\big) = \frac{Q_c^2}{3}\alpha_{\rm em}\frac{m^2_{\chi_{c1}} - m^2_{J/\psi}}{2m_{\chi_{c1}}}\left(|E_1|^2 + |M_2|^2\right). \tag{5}$$

In our computation we use the gauge field configurations produced by the Extended Twisted Mass Collaboration (ETMC) with $N_f = 2+1+1$ dynamical Wilson-Clover twisted mass fermions which guarantees the automatic $O(a)$ improvement of parity-even observables [13,14]. Basic information regarding the four lattice ensembles used in this work is collected in Table 1, and further details can be found in Ref. [15]. For the reasons that will become clear later on, in this work we employ the mixed lattice action, a setup first introduced in Ref. [14] and then further described in Ref. [15]. In other words, in contrast to the sea quarks, the valence quark action is discretized with the so-called Osterwalder–Seiler (OS) regularization, namely,

$$S = \sum_{f=u,d,s,c}\sum_x \bar q_f(x)\Big[\gamma_\mu\bar\nabla_\mu[U] - ir_f\gamma^5(W^{\rm cl}[U] + m_{\rm cr}) + m_f\Big]q_f(x)\,, \tag{6}$$

where $W^{\rm cl}[U]$ is the Wilson-Clover term [16], $m_{\rm cr}$ is the critical mass, m_f the quark mass of the flavor f (with $m_u = m_d = m_l$), and $r_f = \pm 1$ is the sign of the twisted-Wilson parameter for the flavor f. At each lattice spacing, the charm quark mass m_c has been tuned to reproduce $m_{D_s} = 1968$ MeV.

We work in the χ_{c1} rest frame ($\mathbf{p} = 0$). In order to ensure $q^2 = 0$ one needs to give J/ψ a three-momentum

$$|\mathbf{k}| = \frac{m^2_{\chi_{c1}} - m^2_{J/\psi}}{2m_{\chi_{c1}}} \simeq 389.4\ \text{MeV}\,. \tag{7}$$

The form factors E_1 and M_2 can be extracted from the following three-point correlation functions:

$$C^{ijk}_{\rm 3pt}(t_\chi;t_J) = \sum_{\mathbf{x},\mathbf{y},\mathbf{z}} e^{i\mathbf{k}(\mathbf{x}-\mathbf{y})}\left\langle 0\left|\mathcal{O}^i_{J/\psi}(\mathbf{x},0)J^j_{\rm em}(\mathbf{y},-t_J)\mathcal{O}^{k\dagger}_{\chi_{c1}}(\mathbf{z},-t_\chi)\right|0\right\rangle\,, \tag{8}$$

Table 1
$N_f = 2+1+1$ ETMC gauge ensembles used in this work. a is the lattice spacing, L/a spatial extent of the lattice, am_c is the bare charm quark mass and Z_V the vector current renormalization constant [15]. The number of gauge configurations N_g, and the number of (spin and color diluted) stochastic sources N_s employed for the calculation of the relevant two- and three-point correlation functions are also given. With the exception of A48 (which corresponds to a pion mass $m_\pi \simeq 175$ MeV), all the ensembles have been generated at physical values of the light, strange and charm quark masses.

ID	L/a	a fm	Z_V	am_c	N_g	N_s
A48	48	0.0907(5)	0.68700(15)	0.2620	800	140
B64	64	0.07948(11)	0.706354(54)	0.23157	400	32
C80	80	0.06819(14)	0.725440(33)	0.19840	640	24
D96	96	0.056850(90)	0.744132(31)	0.16490	300	35

where $\mathcal{O}^i_{J/\psi}$ and $\mathcal{O}^k_{\chi_{c1}}$ are the interpolating operators of the J/ψ and χ_{c1} mesons,

$$\begin{aligned}\mathcal{O}^i_{J/\psi}(\mathbf{x},t) &= \sum_{\mathbf{y}} \bar{q}_c(\mathbf{x},t) G_t^n(\mathbf{x},\mathbf{y})\gamma^i q_c(\mathbf{y},t),\\ \mathcal{O}^k_{\chi_{c1}}(\mathbf{x},t) &= \sum_{\mathbf{y}} \bar{q}_c(\mathbf{x},t) G_t^n(\mathbf{x},\mathbf{y})\gamma^k\gamma^5 q_c(\mathbf{y},t),\end{aligned} \tag{9}$$

where

$$G_t(\mathbf{x},\mathbf{y}) = \frac{1}{1+6\kappa}\left[\delta_{\mathbf{x},\mathbf{y}} + \kappa H_t(\mathbf{x},\mathbf{y})\right], \tag{10}$$

and $H_t(\mathbf{x},\mathbf{y})$ is the Gaussian smearing operator,

$$H_t(\mathbf{x},\mathbf{y}) = \sum_{\mu=1}^{3}\left[U^\star_\mu(\mathbf{x},t)\delta_{\mathbf{x}+\hat{\mu},\mathbf{y}} + U^{\star\dagger}_\mu(\mathbf{x}-\hat{\mu},t)\delta_{\mathbf{x}-\hat{\mu},\mathbf{y}}\right], \tag{11}$$

with $U^\star_\mu(x)$ being the so-called APE-smeared links, cf. [17]. As in our recent work [18], we used the smearing parameter $\kappa = 0.4$, and fix on each ensemble the number of steps n in Eq. (9) to have a smearing radius $r_0 = a\sqrt{n}/\sqrt{\kappa^{-1}+6} \simeq 0.15$ fm, for both J/ψ and χ_{c1} [19]. The spatial momentum $\mathbf{k}$ is injected along the third spatial direction, $\mathbf{k} = (0,0,|\mathbf{k}|)$. With this choice, the interpolating operators in Eq. (9) are such that $O^{k,\dagger}_{\chi_{c1}}$ creates a χ_{c1} with the polarization vector $\eta^\mu_k = \delta^\mu_k$, for three polarization states $k = 1,2,3$, while $O^i_{J/\psi}$ annihilates a J/ψ with $\epsilon^\mu_i = \delta^\mu_i$ for $i = 1,2$, and with $\epsilon_3 = (\alpha,0,0,\sqrt{1+\alpha^2})$, for the longitudinal polarization $i = 3$, where $\alpha = |\mathbf{k}|/m_{J/\psi}$.

The Wick contractions in Eq. (8) give rise to the quark-connected and disconnected contributions. Just as in our recent work [18], here we also focus on the evaluation of the dominant connected diagram, leaving the evaluation of the disconnected contributions for future work. Clearly, only the charm quark component of the electromagnetic current (J^μ_c) contributes to the connected part of $C^{ijk}_{3\mathrm{pt}}(t_\chi;t_J)$. We use twisted boundary conditions to tune the spatial momentum $\mathbf{k}$ to the value given in Eq. (7). This is implemented by twisting the gauge links $U_\mu(x)$ on which one of the charm quark propagators is computed, namely [20–22]

$$U_\mu(x) \to U^\theta_\mu(x) = e^{ia\theta_\mu/L}U_\mu(x), \quad \theta_\mu = (0,\vec{\theta}), \tag{12}$$

with the twisting-angle $\vec{\theta}$ set to

$$\vec{\theta} = (0,0,\theta^c_z), \qquad \theta^c_z = \frac{L}{\pi}|\mathbf{k}|. \tag{13}$$

We denote by $S_c(x,y)$ and $S^\theta_c(x,y)$ the charm quark propagators evaluated on the background field configurations corresponding to $U_\mu(x)$ and $U^\theta_\mu(x)$, respectively, so that $C^{ijk}_{3\mathrm{pt}}(t_\chi;t_J)$ can be written as:[2]

$$C^{ijk}_{3\mathrm{pt}}(t_\chi,t_J) = 2\sum_{\mathbf{x},\mathbf{y},\mathbf{z}}\left\langle \mathrm{Tr}\left[S_c(x,z)\gamma^k\gamma^5 S_c(z,y)\gamma^j S^\theta_c(y,x)\gamma^i\right]\right\rangle, \tag{14}$$

where $x = (\mathbf{x},0)$, $y = (\mathbf{y},-t_J)$, $z = (\mathbf{z},-t_\chi)$. The trace Tr[…] is taken over the color and Dirac indices, and $\langle\dots\rangle$ indicates the average over the SU(3) gauge field configurations $U_\mu(x)$. The factor of two in Eq. (14) accounts for the contribution of the charge conjugated diagram. The sum over $\mathbf{x}$ is stochastically evaluated by inverting the Dirac charm quark operator on a number N_s of (spin and color diluted) spatial stochastic sources placed at time $t = 0$. The backward propagator $S_c(x,z)$ is then obtained from $S_c(z,x)$ by using γ^5-hermiticity.

2.1. Avoiding the spurious mixing

We now discuss how the charm quark bilinears $\mathcal{O}_{J/\psi}$, $\mathcal{O}_{\chi_{c1}}$, and the current J^μ_c, are discretized on the lattice. When evaluating the connected diagrams using the twisted mass (TM) action, there are different options when it comes to discretizing the quark bilinears and they differ in the choice of the Wilson parameter of the quark field, $r_+ = \pm1$, and of the antiquark field, $r_- = \pm1$. They can be chosen to be opposite ($r_+ = -r_-$) or equal ($r_+ = r_-$). The two regularizations are known as the TM and OS regularizations, respectively. The results obtained using different combinations of TM and OS bilinears differ only by $O(a^2)$ effects. In Ref. [18], we have shown that the TM regularization of the h_c interpolating operator ($J^{PC} = 1^{+-}$) is protected from mixing with $J^{PC} = 1^{--}$ and 1^{++} states. This is so because in the TM regularization the product between parity P and G-parity G, is an exact lattice symmetry, which is then sufficient to exclude the aforementioned mixing. In the case at hand, instead, the exact $P\times G$ symmetry is not sufficient to exclude the mixing between 1^{++} and 1^{--} states. Indeed, when using the TM regularization the corresponding interpolating operator $O^{k\dagger}_{\chi_{c1}}$ also creates vector states, as we numerically illustrate in Section 3. In the OS regularization ($r_+ = r_-$), however, one can use the exact invariance under charge conjugation C, which in our case forbids the creation of states $J^{PC} = 1^{--}$ and $J^{PC} = 1^{+-}$ when using the interpolating operators $O^{k\dagger}_{\chi_{c1}}$, thus representing a favorable regularization.

On the basis of the considerations made above, we therefore employ the OS regularization both for interpolating fields $O_{\chi_{c1}}$, $O_{J/\psi}$, and for the electromagnetic current.[3] With this choice, the renormalization constant of the local electromagnetic current is given by $Z_V(g_0^2)$, the values of which are given in Table 1. For a comprehensive discussion on bilinear interpolators in twisted mass lattice QCD see Ref. [23].

2.2. Extraction of the form factors E_1 and M_2

We first need to consider the two point functions of interpolating fields $\mathcal{O}^i_{J/\psi}$ and $\mathcal{O}^j_{\chi_{c1}}$, respectively, in order to extract their mass/energy and their couplings:

$$\begin{aligned}C^i_{2,J/\psi}(t) &= \sum_{\mathbf{x}} e^{i\mathbf{kx}}\left\langle 0\middle|\mathcal{O}^i_{J/\psi}(\mathbf{x},t)\mathcal{O}^{i\dagger}_{J/\psi}(\mathbf{0},0)\middle|0\right\rangle,\\ C^k_{2,\chi_{c1}}(t) &= \sum_{\mathbf{x}}\left\langle 0\middle|\mathcal{O}^k_{\chi_{c1}}(\mathbf{x},t)\mathcal{O}^{k\dagger}_{\chi_{c1}}(\mathbf{0},0)\middle|0\right\rangle,\end{aligned} \tag{15}$$

in which, as before, we neglect the Zweig suppressed disconnected contributions. In the limit of large Euclidean time t, the two point correlation functions behave as:

$$\begin{aligned}C^i_{2,J/\psi}(t) &= \frac{\left|Z^i_{J/\psi}\right|^2}{2E_{J/\psi}}\left(e^{-E_{J/\psi}t} + e^{-E_{J/Psi}(T-t)}\right) + \dots,\\ C^k_{2,\chi_{c1}}(t) &= \frac{\left|Z^k_{\chi_{c1}}\right|^2}{2m_{\chi_{c1}}}\left(e^{-m_{\chi_{c1}}t} + e^{-m_{\chi_{c1}}(T-t)}\right) + \dots\ ,\end{aligned} \tag{16}$$

where $m_{\chi_{c1}}$ and $E_{J/\psi}$ are the mass and energy of the corresponding ground states, and

$$\begin{aligned}Z^i_{J/\psi} &= \left\langle 0\middle|\mathcal{O}^i_{J/\psi}\middle|J/\psi(k,\epsilon_i)\right\rangle,\\ Z^k_{\chi_{c1}} &= \left\langle \chi_{c1}(p,\eta_k)\middle|\mathcal{O}^{k\dagger}_{\chi_{c1}}\middle|0\right\rangle.\end{aligned} \tag{17}$$

The ellipses in Eq. (16) denote contributions that vanish in the large time limit, $0 \ll t \ll T$, and are further suppressed by the smearing, cf. Eq. (10). We also calculated $C^i_{2,J/\psi}(t)$ with $\mathbf{k} = \mathbf{0}$, in order to extract $m_{J/\psi}$. Clearly, with our choice of kinematics we have: $Z^1_{\chi_{c1}} = Z^2_{\chi_{c1}} = Z^3_{\chi_{c1}}$, and $Z^1_{J/\psi} = Z^2_{J/\psi}$.

[2] To simplify the expressions we consider the case of local interpolating operators, i.e. $\kappa = 0$. In the computations, however, we implemented the smearing in a way discussed in the text.

[3] When using the OS regularization for the J/ψ interpolating operator, it is possible that $J^{PC} = 1^{+-}$ states are created, however, being heavier than the J/ψ they do not represent an obstacle to our computation.

It is then straightforward to use Eq. (3) and combine the above quantities into

$$\overline{E}_1(t_\chi;t_J) = \frac{iZ_V(g_0^2)}{\sqrt{2}Q_c} 4\,E_{J/\psi}\; e^{E_{J/\psi}t_J}\; e^{m_{\chi_{c1}}(t_\chi - t_J)} \times \left[\frac{C_{3\mathrm{pt}}^{213}(t_\chi;t_J)}{Z_{J/\psi}^2 Z_{\chi_{c1}}^3} - \frac{C_{3\mathrm{pt}}^{312}(t_\chi;t_J)}{Z_{J/\psi}^3 Z_{\chi_{c1}}^2} \right],$$

$$\overline{M}_2(t_\chi;t_J) = \frac{iZ_V(g_0^2)}{\sqrt{2}Q_c} 4\,E_{J/\psi}\; e^{E_{J/\psi}t_J}\; e^{m_{\chi_{c1}}(t_\chi - t_J)} \times \left[\frac{C_{3\mathrm{pt}}^{213}(t_\chi;t_J)}{Z_{J/\psi}^2 Z_{\chi_{c1}}^3} + \frac{C_{3\mathrm{pt}}^{312}(t_\chi;t_J)}{Z_{J/\psi}^3 Z_{\chi_{c1}}^2} \right], \tag{18}$$

which, for large Euclidean time separations, yield the desired form factors E_1 and M_2, namely,

$$\overline{E}_1(t_\chi;t_J) \xrightarrow[t_\chi - t_J \to \infty]{t_J \to \infty} E_1\,,$$

$$\overline{M}_2(t_\chi;t_J) \xrightarrow[t_\chi - t_J \to \infty]{t_J \to \infty} M_2\,. \tag{19}$$

Note that in $C_{3\mathrm{pt}}^{ijk}(t_\chi;t_J)$ the interpolating field of J/ψ is placed at $t=0$, the charm quark component of the electromagnetic current is then inserted into a charm quark line at a fixed $-t_J < 0$, while the time $-t_\chi \ll -t_J$, at which the χ_{c1} is created, corresponds to the *sink* of the correlation function is free. This allows us to carefully monitor the onset of dominance of the χ_{c1} state. Since in our computational setup the time t_J is fixed, we must choose it to be large enough to be able to isolate the J/ψ state. The advantage of placing the interpolator corresponding to J/ψ at the source of the correlation function is that t_J can be chosen reasonably large since the signal-to-noise ratio (S/N) of $C_{3\mathrm{pt}}^{ijk}(t_\chi;t_J)$ for fixed $|t_\chi - t_J|$ decreases only as $e^{-(E_{J/\psi}-m_{\eta_c})} \simeq e^{-\Delta_c t}$, where $\Delta_c \simeq 113$ MeV is the hyperfine splitting. As will be detailed in the next subsection, we have considered two different values of $t_J \simeq 1.6, 2.4$ fm, and observed only tiny differences in our results that we nevertheless include in the final systematic error.

3. Numerical results

In Fig. 1 we show the effective mass of the two-point function $C_{2,\chi_{c1}}^k(t)$ regularized in both the TM (blue diamond) and OS (red squares) regularizations, as well as the effective mass of $C_{2,J/\psi}^i(t)$ (for $|\mathbf{k}|=0$) in the OS regularization (magenta squares). The results correspond to our ensemble B64. We clearly see that with the TM regularization the function $C_{2,\chi_{c1}}^k(t)$ exhibits mixing with J/ψ. However, due to the exact C-symmetry, such spurious mixing is absent when using the OS regularization which is why, in this work, we use that regularization for the valence quarks.

In Fig. 2 we show the effective mass plots for J/ψ and χ_{c1} mesons, for all four of our lattices.

We should emphasize that the charm quark mass has been fixed by $m_{D_s} = 1968$ MeV at each value of the lattice spacing, and due to the finite lattice artefacts the values of $m_{J/\psi}$ and $m_{\chi_{c1}}$ are not the same for all ensembles. Owing to the fact that the S/N ratio of $C_{2,J/\psi}^i(t)$ decreases only as $e^{-\Delta_c t}$, the quality of the plateaus for J/ψ are excellent. In the case of $C_{2,\chi_{c1}}(t)$ the S/N ratio decreases faster but since we use the smeared sources, as well as a large number of gauge configurations and stochastic sources, we are still able to obtain the long plateaus and extract $m_{\chi_{c1}}$ with a very good accuracy. Note that a larger error for the A48 ensemble in Fig. 2 is due to uncertainty on the lattice spacing of that ensemble ($\simeq 0.6\,\%$). The extrapolation to the continuum of the lattice results for $m_{J/\psi}$ and $m_{\chi_{c1}}$ is shown in Fig. 3.

Since there are no signals of a^4 effects in the data, the continuum limit is reached through a simple linear fit in a^2 and for our final results we have:

$$m_{J/\psi} = 3.1052(95)\ \mathrm{GeV}, \qquad m_{\chi_{c1}} = 3.521(12)\ \mathrm{GeV}, \tag{20}$$

in good agreement with the current experimental values, $m_{J/\psi}^{\mathrm{exp}} = 3.096900(6)$ GeV and $m_{\chi_{c1}}^{\mathrm{exp}} = 3.51067(5)$ GeV [7]. These results also suggest that the impact of neglected disconnected (annihilation) contributions is indeed small, at most of the order of our statistical uncertainty which is about $(0.3 \div 0.4)\%$ for both masses.

We now focus on the determination of the form factors E_1 and M_2. At finite lattice spacing we tune the three-momentum $\mathbf{k}$ to the value indicated in Eq. (7) but by using the experimental values of $m_{J/\psi}$ and

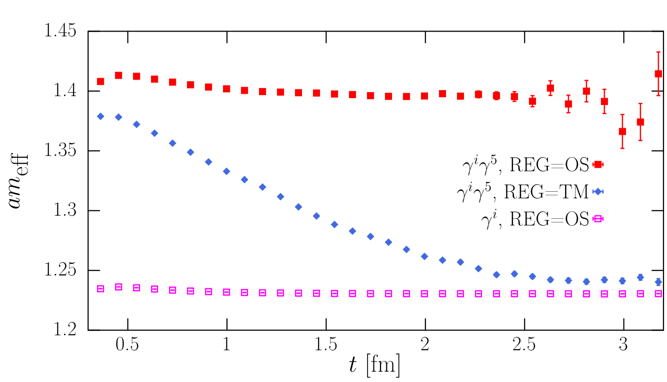

Fig. 1. Effective mass extracted from $C_{2,\chi_{c1}}^k(t)$ in the TM (blue diamonds) and OS (red squares) regularizations, along with the one extracted from $C_{2,J/\psi}^i(t)$ (with $|\mathbf{k}|=0$) in the OS regularization (magenta squares). The data refer to the ensemble B64. (For interpretation of the references to colour in this figure legend, the reader is referred to the web version of this article.)

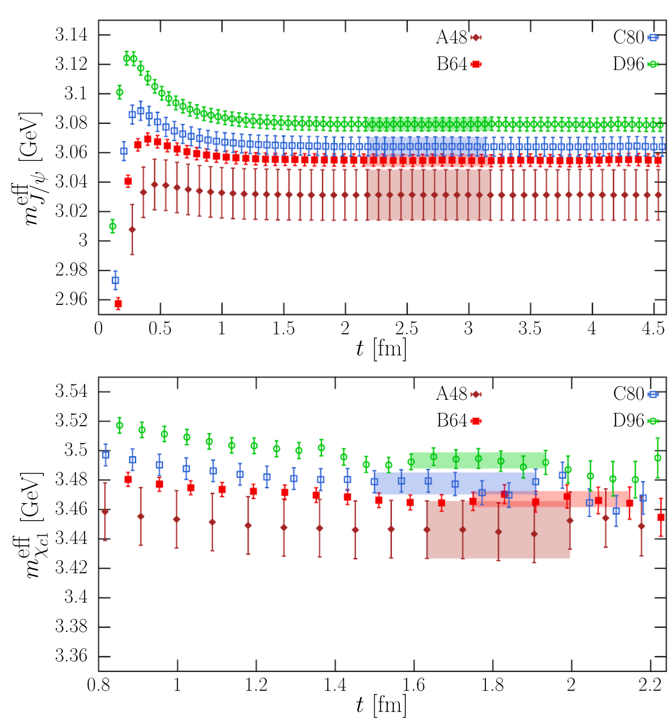

Fig. 2. Effective mass of J/ψ and χ_{c1} for all four gauge ensembles used in this work. The colored bands correspond to our estimate of mass on each ensemble.

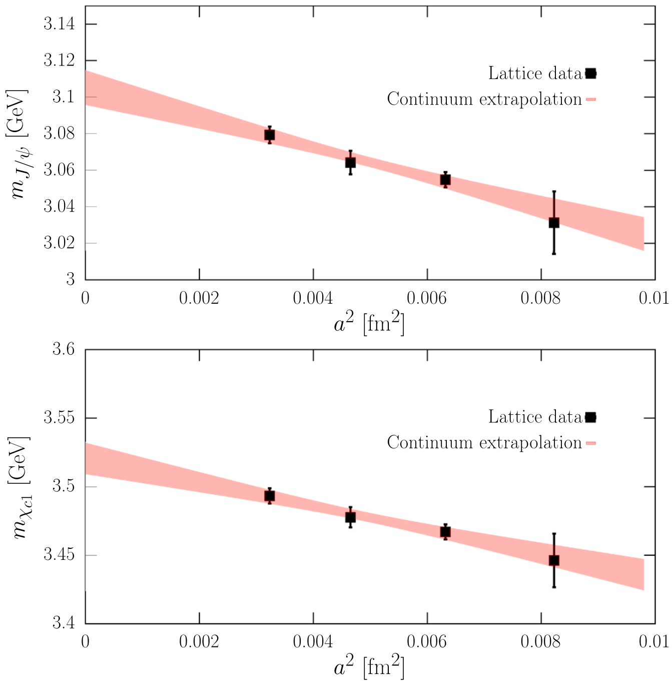

Fig. 3. Extrapolation of $m_{J/\psi}$ and $m_{\chi_{c1}}$ to the continuum limit ($a \to 0$). The colored bands correspond to the best fit obtained after performing a linear extrapolation in a^2. The reduced χ^2 of the two fits is below one.

$m_{\chi_{c1}}$, and not those obtained on the lattice at fixed lattice spacing. The two choices merely amount to a redefinition of the $O(a^2)$ effects because, as we have just shown, our values of the masses in the continuum limit are in full agreement with the experimental ones. In practice, the use of the ensemble values of the masses in Eq. (7) would have produced on the coarsest lattice spacing a variation of the three-momentum $\mathbf{k}$ by less than 1 %, which besides being only an $O(a^2)$ effect, is also completely negligible at the current level of accuracy.

As already anticipated in the previous Section, we keep the time $-t_J$ of the transition operator in $C^{ijk}_{3\mathrm{pt}}(t_\chi; t_J)$ fixed, while t_χ runs over the lattice. It is thus important to choose sufficiently large t_J in order to ensure the dominance of J/ψ. We tested that issue on the B64 ensemble by computing $C^{ijk}_{3\mathrm{pt}}(t_\chi; t_J)$ for two different $t_J \sim 1.6, 2.4$ fm. In Fig. 4 we compare the corresponding $\overline{E}_1(t_\chi; t_J)$ and $\overline{M}_2(t_\chi; t_J)$, cf. Eq. (18). The two results are in good agreement, and only in the case of E_1 we do see an $O(1\sigma)$ difference between the results obtained at the two values of t_J. On the basis of these observations we decided to fix $t_J \simeq 1.7$ fm for all other ensembles, and include, before the continuum extrapolation, a systematic uncertainty ΔE_1 and ΔM_2 to all our results, estimated as:

$$\Sigma_F = |F(t_J \simeq 2.4\ \mathrm{fm}) - F(t_J \simeq 1.6\ \mathrm{fm})| \,,$$
$$\Delta F = \Sigma_F \cdot \mathrm{erf}\left(\frac{\Sigma_F}{\sqrt{2}\sigma_{\Sigma_F}}\right), \qquad F = E_1, M_2 \,, \tag{21}$$

where σ_{Σ_F} is the statistical error of Σ_F and $\mathrm{erf}(x)$ is the error function. The quantities ΔE_1 and ΔM_2 are thus the observed spreads, weighted by the probability that they are not due to statistical fluctuations.

In Fig. 5 we show $\overline{E}_1(t_\chi; t_J)$ and $\overline{M}_2(t_\chi; t_J)$ for all our lattices.[4] For the electric form factor E_1 the cut-off effects are small, of the order of a few percent, in addition to the statistical uncertainties that are $O(1 \div 2\,\%)$). For the magnetic form factor M_2, instead, we observe the

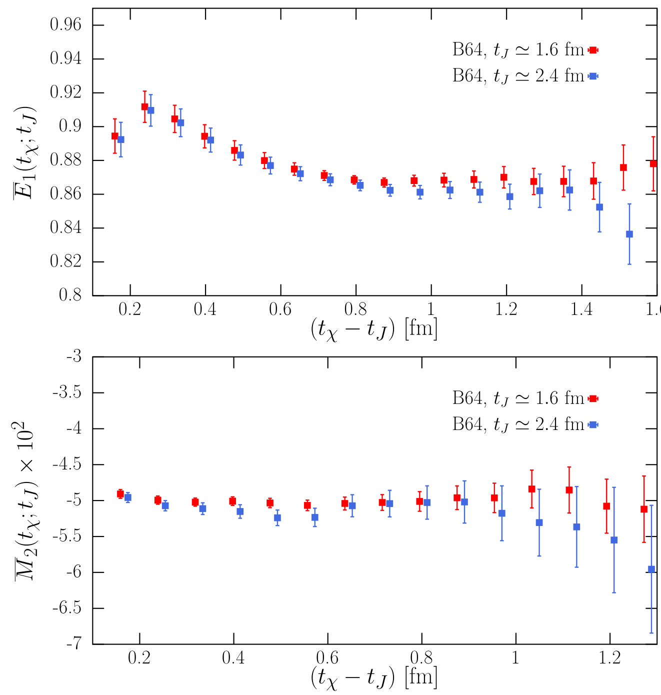

Fig. 4. Comparison between $\overline{E}_1(t_\chi, t_J)$ (left plot) and $\overline{M}_2(t_\chi, t_J)$ (right plot) with $t_J \simeq 1.6$ fm (red) and with $t_J \simeq 2.4$ fm (blue) on the B64 ensemble. The data-points at $t_J \simeq 2.4$ fm have been slightly shifted horizontally for easier comparison. (For interpretation of the references to colour in this figure legend, the reader is referred to the web version of this article.)

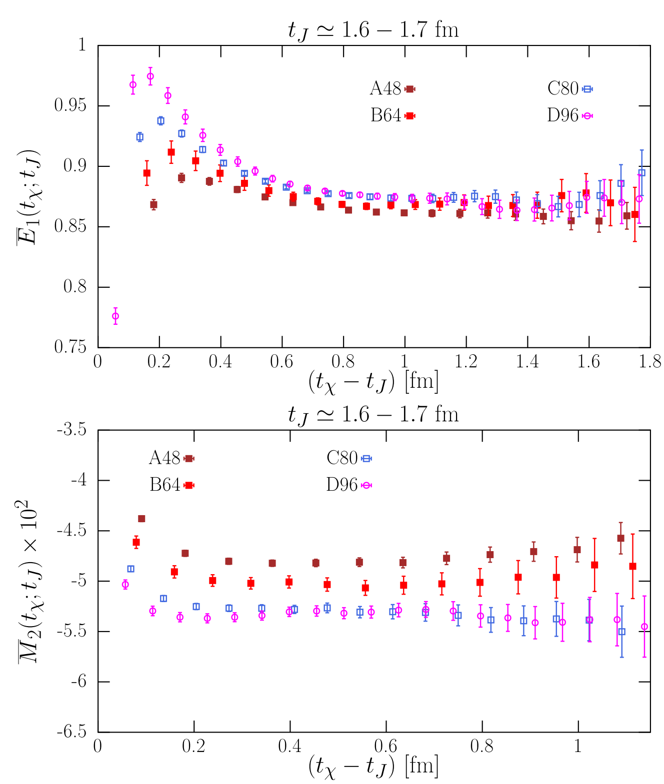

Fig. 5. The functions $\overline{E}_1(t_\chi; t_J)$ (left) and $\overline{M}_2(t_\chi; t_J)$ (right) defined in Eq. (18), as obtained for all lattice ensembles, cf. Table 1, and for t_J fixed as discussed in the text.

[4] For the A48 and D96 ensemble we have averaged the estimators for the form factors in Eq. (18) with the equivalent estimators obtained using the second component J^2_{em} of the electromagnetic current.

Table 2
Values of the form factors E_1 and M_2 for each gauge ensemble used in this study.

a [fm]	0.0907 (5)	0.07948 (11)	0.06819 (14)	0.056850 (90)
E_1	0.8609(60)	0.8686(72)	0.8738(64)	0.8699(74)
$-M_2$	0.04741(72)	0.0502(11)	0.0535(11)	0.0535(12)

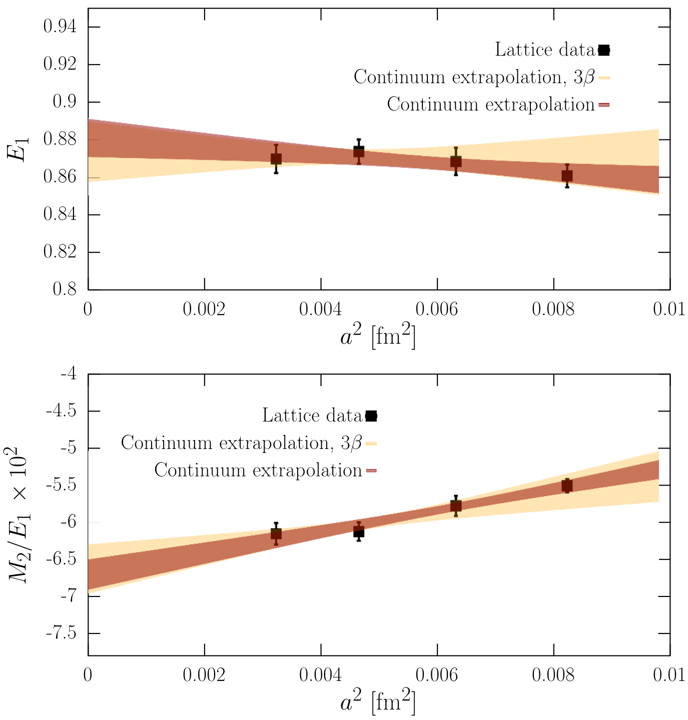

Fig. 6. Continuum-limit extrapolation of the form factor E_1 (top) and of the ratio M_2/E_1 (bottom). The coloured bands in dark red correspond to the best-fit function obtained after performing a linear fit in a^2 to our lattice data. The reduced χ^2 of the fit is about 0.3 and 0.9 for E_1 and M_2/E_1, respectively. The orange bands in the figures correspond instead to the linear fits performed excluding the data at the coarsest lattice spacing. (For interpretation of the references to colour in this figure legend, the reader is referred to the web version of this article.)

larger cut-off effects $O(10-15\,\%)$ that dominate the tiny statistical errors. Note also that the onset of the plateau region occurs already at small times, ~ 0.5 fm. The form factors are then merely obtained from the fit to a constant.

Our values for E_1 and M_2 are presented in Table 2, which we then extrapolate to the continuum limit using a simple linear a^2 fit, cf. Fig. 6. The corresponding $\chi^2/\mathrm{dof} \simeq 0.3$ for E_1, and $\chi^2/\mathrm{dof} \simeq 0.9$ for the ratio M_2/E_1 are satisfactory. To estimate the systematic error associated to the continuum limit extrapolation we have performed a second linear fit excluding the data at the coarsest lattice spacing. The corresponding fits are shown in Fig. 6 as orange bands. Our final results, obtained by averaging the two different type of fits using the Bayesian Akaike Information Criterion[5] (BAIC) read:

$$\boxed{E_1 = 0.879(11), \qquad \frac{M_2}{E_1} = -0.0668(22).} \tag{22}$$

Note that our E_1 has an uncertainty of about 1.2 %, while the uncertainty of the ratio M_2/E_1 is about 3 %. We now compare our results with existing experimental data as well as with previous lattice results.

[5] For more details on the BAIC procedure adopted, we refer to the discussion around Eqs. (21)-(22) of Ref. [18].

4. Comparison with existing experimental and lattice results

After inserting our results Eq. (22) into Eq. (5) we obtain

$$\Gamma(\chi_{c1} \to J/\psi\,\gamma) = 0.3265(79)\ \mathrm{MeV}, \tag{23}$$

where we used $\alpha_{\mathrm{em}}^{-1} = 137.036$. The decay rate is dominated by the electric dipole form factor E_1, while the contribution of M_2 is negligible compared to E_1 at the current level of precision. Our result is 1.1σ larger than the experimental value $\Gamma(\chi_{c1} \to J/\psi\,\gamma)^{\mathrm{exp}} = 0.302(21)$ MeV, which we obtain by combining $\mathcal{B}(\chi_{c1} \to J/\psi\gamma)^{\mathrm{exp}} = (34.3 \pm 1.3)\%$ [7] with the PDG average $\Gamma(\chi_{c1}) = 0.88(5)$ MeV [7]. If, instead, we use $\Gamma(\chi_{c1}) = 0.84(4)$ MeV, as suggested by the global PDG fit, we would have $\Gamma(\chi_{c1} \to J/\psi\,\gamma)^{\mathrm{exp}} = 0.288(18)$ MeV, which is 2σ lower than our result Eq. (23). We emphasize that $\Gamma(\chi_{c1} \to J/\psi\,\gamma)$ has only been measured by the Fermilab E835 Collaboration [6]. An independent measurement by BES III would be very welcome. The difference might be also due to disconnected contributions which were omitted in our computation and will be addressed elsewhere.

As already mentioned in Introduction, the only two existing lattice QCD results have been obtained either at a single lattice spacing in the quenched approximation [11] or with two lattice spacings and by including $N_f = 2$ (unphysical) dynamical light quarks [12]. With respect to $\Gamma(\chi_{c1} \to J/\psi\,\gamma) = 0.270(70)$ MeV, reported in Ref. [11], our

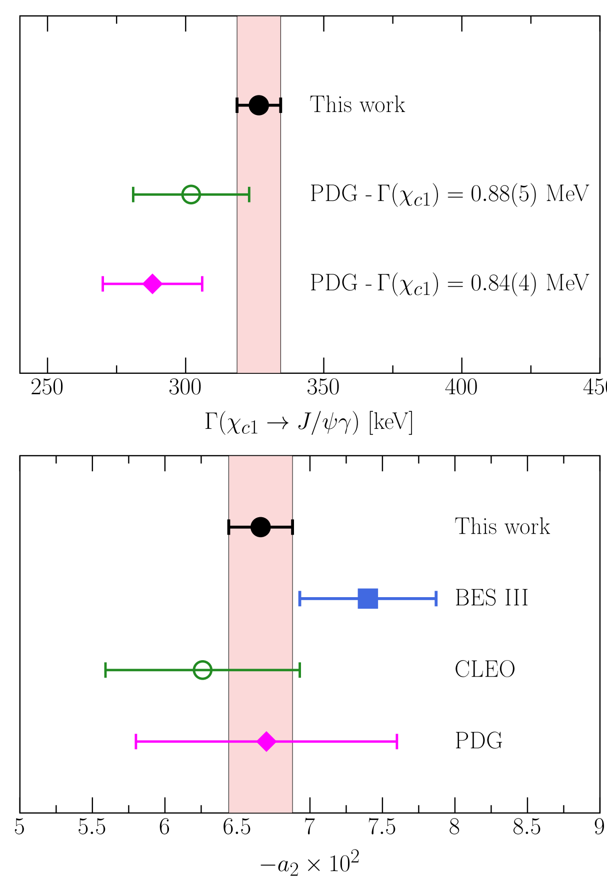

Fig. 7. Comparison between our results and experimental ones. In the upper panel our value for $\Gamma(\chi_{c1} \to J/\psi\,\gamma)$ (filled black circle) is shown alongside the value obtained by the PDG [7] using the average value $\Gamma(\chi_{c1}) = 0.88(5)$ MeV (empty green circle) and the PDG global fit result $\Gamma(\chi_{c1}) = 0.84(4)$ MeV (filled magenta diamond). In the lower panel we compare our estimate of a_2 (filled black circle) with the measurement by BES III [9] (filled blue square) and CLEO [8] (empty green circle), as well as with the PDG average [7] (filled magenta diamond). (For interpretation of the references to colour in this figure legend, the reader is referred to the web version of this article.)

result Eq. (23) can be viewed as a substantial improvement. On the other hand, our result is much larger than $\Gamma(\chi_{c1} \to J/\psi\,\gamma) = 0.070(20)$ MeV, obtained at finer of the two lattice spacings considered in Ref. [12]. We suspect that the small decay width reported in Ref. [12] is a consequence of using the TM regularization for the χ_{c1} interpolating field. As can be seen in Fig. 1 of Ref. [12], the interpolator they adopted has a clear overlap with the J/ψ meson.

The quantity a_2, defined in Eq. (1), can now easily be evaluated from our form factor ratio Eq. (22). We have:

$$a_2 = -0.0666(22)\,. \tag{24}$$

That same quantity is experimentally accessible through the angular distribution analysis of the decay chain $e^+e^- \to \psi(nS) \to \chi_{c1}\gamma$ followed by $\chi_{c1} \to J/\psi\,\gamma \to e^+e^-\gamma$, cf. Refs. [24–26] and Refs. [8,9]. The experimental average, $a_2^{\rm exp} = -0.067(9)$ [7], is in remarkable agreement with our result Eq. (22). This can be viewed as a very fine verification of the validity of the lattice QCD approach when it comes to the precision computation of hadronic quantities. The only other lattice QCD determination of this quantity was reported in [11], where $a_2 = -0.09(7)$ and $a_2 = -0.20(6)$ were quoted, reflecting the ambiguity in extrapolating the form factors to $q^2 = 0$, i.e., whether they are extrapolated separately and then combined in a ratio, or whether the ratio $M_2(q^2)/E_1(q^2)$ is directly extrapolated to $q^2 = 0$. Our result for a_2 thus represents a very significant improvement in precision, by more than an order of magnitude. In Fig. 7 we show a comparison between our results Eq. (22) and the available experimental values.

5. Conclusions

In this paper we provide the first full QCD computation of the hadronic matrix element relevant to the $\chi_{c1} \to J/\psi\,\gamma$ decay by employing the gauge field configurations produced by the ETMC with $N_f = 2+1+1$ Wilson-Clover twisted-mass quarks. A delicate point in this project was to avoid the spurious mixing with operators of the opposite parity which can plague the analysis when using the TM regularization. Using the OS regularization for the valence quarks solves this problem and the lowest lying state coupling to the $J^{PC} = 1^{++}$ interpolating field operator is indeed χ_{c1}, and not J/ψ which is lighter and corresponds to $J^{PC} = 1^{--}$. This is so because the OS regularization preserves the charge conjugation. We checked that feature numerically and showed that the OS valence regularization indeed provides favorable conditions for the computation of our hadronic matrix element. To ensure that the photon is on-shell ($q^2 = 0$) we tuned the twisted boundary conditions to one of the charm quark propagators in such a way that it actually gives a desired three-momentum to the daughter meson, J/ψ. In addition to the dominant electric dipole form factor E_1, due to the high statistics of the four gauge ensembles used in this work, we were also able to compute the ratio of the magnetic quadrupole form factor M_2 and E_1. We checked the smooth scaling of our results with the squared lattice spacing (a^2) and then extrapolated them to the continuum limit. Our final results are given in Eq. (22) which represent a significant improvement compared to the previous lattice studies. Our results give a decay rate that is about $(1 \div 2)\sigma$ larger than the one inferred from the experimental measurements, assuming that the full width of χ_{c1} is the one provided in Ref. [7], which still needs to be confirmed by BES III.

The more recent experiments focused on a detailed angular analysis of this decay, allowing one to extract a_2, the quantity that measures the amount of the (suppressed) magnetic quadrupole contribution to the decay amplitude, relative to the (dominant) electric dipole one. Our result is in agreement with the experimental ones, and it could be seen as strong confirmation of the validity of the lattice QCD approach when dealing with the requirement of high precision for hadronic quantities.

Throughout this computation, we did not account for the disconnected diagrams. Being either Zweig or SU(3) suppressed, these contributions are expected to be tiny. However, this should be verified through direct computation, which is a direction we plan to explore in the near future.

6. Acknowledgments

We thank the ETMC for the most enjoyable collaboration. V.L., F.S., G.G., R.F., and N.T. are supported by the Italian Ministry of University and Research (MUR) and the European Union (EU) - Next Generation EU, Mission 4, Component 1, PRIN 2022, CUP F53D23001480006. F.S. is supported by ICSC - Centro Nazionale di Ricerca in High Performance Computing, Big Data and Quantum Computing, funded by European Union - Next Generation EU and by Italian Ministry of University and Research (MUR) projects FIS_00001556 and PRIN_2022N4W8WR. We acknowledge support from the LQCD123, ENP, and SPIF Scientific Initiatives of the Italian Nuclear Physics Institute (INFN). This project has received support from the IN2P3 (CNRS) Master Project HighPTflavor.

The open-source packages tmLQCD [27–30], LEMON [31], DD-αAMG [32–35], QPhiX [36,37] and QUDA [38–40] have been used in the ensemble generation.

We gratefully acknowledge the ICSC - Centro Nazionale di Ricerca in High Performance Computing for providing computing time under the allocations RAC 1916318. We gratefully acknowledge CINECA for the provision of GPU time on Leonardo supercomputing facilities under the specific initiative INFN-LQCD123, and under project IscrB VITO-QCD and project IscrB SemBD. We gratefully acknowledge EuroHPC Joint Undertaking for awarding us access to MareNostrum5 through the project EHPC-EXT-2024E01-031. The authors gratefully acknowledge the Gauss Centre for Supercomputing e.V. (https://www.gauss-centre.eu) for funding this project by providing computing time on the GCS Supercomputers SuperMUC-NG at Leibniz Supercomputing Centre. The authors acknowledge the Texas Advanced Computing Center (TACC) at The University of Texas at Austin for providing HPC resources (Project ID PHY21001). We gratefully acknowledge PRACE for awarding access to HAWK at HLRS within the project with Id Acid 4886. We acknowledge the Swiss National Supercomputing Centre (CSCS) and the EuroHPC Joint Undertaking for awarding this project access to the LUMI supercomputer, owned by the EuroHPC Joint Undertaking, hosted by CSC (Finland) and the LUMI consortium through the Chronos programme under project IDs CH17-CSCS-CYP. We acknowledge EuroHPC Joint Undertaking for awarding the project ID EHPC-EXT-2023E02-052 access to MareNostrum5 hosted by at the Barcelona Supercomputing Center, Spain. We also thank the GENCI.fr for granting us access to the Jean Zay computers of the computing center IDRIS in Orsay.

Data availability

Data will be made available on request.

Declaration of competing interest

The authors declare that they have no known competing financial interests or personal relationships that could have appeared to influence the work reported in this paper.

References

[1] G.T. Bodwin, E. Braaten, G.P. Lepage, Rigorous QCD analysis of inclusive annihilation and production of heavy quarkonium, Phys. Rev. D 51 (1995) 1125–1171. [Erratum: Phys.Rev.D 55, 5853 (1997)]. hep-ph/9407339. https://doi.org/10.1103/PhysRevD.55.5853

[2] N. Brambilla, A. Pineda, J. Soto, A. Vairo, Potential NRQCD: an effective theory for heavy quarkonium, Nucl. Phys. B 566 (2000) 275. hep-ph/9907240. https://doi.org/10.1016/S0550-3213(99)00693-8

[3] S. Fleming, I.Z. Rothstein, A.K. Leibovich, Power counting and effective field theory for charmonium, Phys. Rev. D 64 (2001) 036002. hep-ph/0012062. https://doi.org/10.1103/PhysRevD.64.036002

[4] N. Brambilla, A. Pineda, J. Soto, A. Vairo, Effective field theories for heavy quarkonium, Rev. Mod. Phys. 77 (2005) 1423. hep-ph/0410047. https://doi.org/10.1103/RevModPhys.77.1423

[5] T.A. Armstrong, et al., E760, Study of the χ_1 and χ_2 charmonium states formed in $\bar{p}p$ annihilations, Nucl. Phys. B 373 (1992) 35–54. https://doi.org/10.1016/0550-3213(92)90448-K

[6] M. Andreotti, et al., Measurement of the resonance parameters of the $\chi_1(1^3P_1)$ and $\chi_2(1^3P_2)$ states of charmonium formed in $p\bar{p}$ annihilations, Nucl. Phys. B 717 (2005) 34–47. hep-ex/0503022. https://doi.org/10.1016/j.nuclphysb.2005.03.042

[7] S. Navas, et al., Particle Data Group, Review of particle physics, Phys. Rev. D 110 (3) (2024) 030001. https://doi.org/10.1103/PhysRevD.110.030001

[8] M. Artuso, et al., CLEO, Higher-order multipole amplitudes in charmonium radiative transitions, Phys. Rev. D 80 (2009) 112003. 0910.0046. https://doi.org/10.1103/PhysRevD.80.112003

[9] M. Ablikim, et al., BESIII, Measurement of higher-order multipole amplitudes in $\psi(3686) \to \gamma\chi_{c1,2}$ with $\chi_{c1,2} \to \gamma J/\psi$ and search for the transition $\eta_c(2S) \to \gamma J/\psi$, Phys. Rev. D 95 (7) (2017) 072004. 1701.01197. https://doi.org/10.1103/PhysRevD.95.072004

[10] J.J. Dudek, R.G. Edwards, D.G. Richards, Radiative transitions in charmonium from lattice QCD, Phys. Rev. D 73 (2006) 074507. hep-ph/0601137. https://doi.org/10.1103/PhysRevD.73.074507

[11] J.J. Dudek, R. Edwards, C.E. Thomas, Exotic and excited-state radiative transitions in charmonium from lattice QCD, Phys. Rev. D 79 (2009) 094504. 0902.2241. https://doi.org/10.1103/PhysRevD.79.094504

[12] N. Li, H. Su, Y.-J. Wu, $\chi_{c1} \to J/\psi\gamma$ Decay width on $N_f = 2$ twisted mass lattice QCD, Eur. Phys. J. A 58 (7) (2022) 122. https://doi.org/10.1140/epja/s10050-022-00768-w

[13] R. Frezzotti, G.C. Rossi, Chirally improving Wilson fermions. 1. o(a) improvement, JHEP 08 (2004) 007. hep-lat/0306014. https://doi.org/10.1088/1126-6708/2004/08/007

[14] R. Frezzotti, G.C. Rossi, Chirally improving Wilson fermions. II. four-quark operators, JHEP 10 (2004) 070. hep-lat/0407002. https://doi.org/10.1088/1126-6708/2004/10/070

[15] C. Alexandrou, et al., Extended Twisted Mass Collaboration (ETMC), strange and charm quark contributions to the muon anomalous magnetic moment in lattice QCD with twisted-mass fermions (2024). 2411.08852

[16] B. Sheikholeslami, R. Wohlert, Improved continuum limit lattice action for QCD with Wilson fermions, Nucl. Phys. B 259 (1985) 572. https://doi.org/10.1016/0550-3213(85)90002-1

[17] D. Becirevic, F. Sanfilippo, Lattice QCD study of the radiative decays $J/\psi \to \eta_c\gamma$ and $h_c \to \eta_c\gamma$, JHEP 01 (2013) 028. 1206.1445. https://doi.org/10.1007/JHEP01(2013)028

[18] D. Bečirević, R. Di Palma, R. Frezzotti, G. Gagliardi, V. Lubicz, F. Sanfilippo, N. Tantalo, Lattice QCD determination of the radiative decay rates $h_c \to \eta_c\gamma$ and $h_b \to \eta_b\gamma$ (2025). 2504.16807[hep-lat]

[19] R. Di Palma, G. Gagliardi, F. Sanfilippo, Investigation of optimal smearing for mesons, PoS LATTICE2023 (2024) 152. https://doi.org/10.22323/1.453.0152

[20] G.M. de Divitiis, R. Petronzio, N. Tantalo, On the discretization of physical momenta in lattice QCD, Phys. Lett. B 595 (2004) 408–413. hep-lat/0405002. https://doi.org/10.1016/j.physletb.2004.06.035

[21] P.F. Bedaque, Aharonov-Bohm effect and nucleon nucleon phase shifts on the lattice, Phys. Lett. B 593 (2004) 82–88. nucl-th/0402051. https://doi.org/10.1016/j.physletb.2004.04.045

[22] C.T. Sachrajda, G. Villadoro, Twisted boundary conditions in lattice simulations, Phys. Lett. B 609 (2005) 73–85. hep-lat/0411033. https://doi.org/10.1016/j.physletb.2005.01.033

[23] R.G. Petry, D. Harnett, R. Lewis, R.M. Woloshyn, Exploring the meson spectrum with twisted mass lattice QCD, Phys. Rev. D 78 (2008) 074502. 0803.4141. https://doi.org/10.1103/PhysRevD.78.074502

[24] J.L. Rosner, M2 signatures in psi(2S) radiative decays, Phys. Rev. D 78 (2008) 114011. 0809.0471. https://doi.org/10.1103/PhysRevD.78.114011

[25] K.J. Sebastian, H. Grotch, F.L. Ridener, Multipole amplitudes in parity changing one photon transitions of charmonium, Phys. Rev. D 45 (1992) 3163–3172. https://doi.org/10.1103/PhysRevD.45.3163

[26] G. Karl, S. Meshkov, J.L. Rosner, Quark magnetic moments and E1 radiative transitions in charmonium, Phys. Rev. Lett. 45 (1980) 215. https://doi.org/10.1103/PhysRevLett.45.215

[27] K. Jansen, C. Urbach, TmLQCD: a program suite to simulate Wilson twisted mass lattice QCD, Comput. Phys. Commun. 180 (2009) 2717–2738. 0905.3331. https://doi.org/10.1016/j.cpc.2009.05.016

[28] A. Abdel-Rehim, F. Burger, A. Deuzeman, K. Jansen, B. Kostrzewa, L. Scorzato, C. Urbach, Recent developments in the tmLQCD software suite, PoS LATTICE2013 (2014) 414. 1311.5495. https://doi.org/10.22323/1.187.0414

[29] A. Deuzeman, K. Jansen, B. Kostrzewa, C. Urbach, Experiences with openMP in tmLQCD, PoS LATTICE2013 (2014) 416. 1311.4521. https://doi.org/10.22323/1.187.0416

[30] B. Kostrzewa, S. Bacchio, J. Finkenrath, M. Garofalo, F. Pittler, S. Romiti, C. Urbach, ETM, Twisted mass ensemble generation on GPU machines, PoS LATTICE2022 (2023) 340. 2212.06635. https://doi.org/10.22323/1.430.0340

[31] A. Deuzeman, S. Reker, C. Urbach, ETM, Lemon: an MPI parallel i/o library for data encapsulation using LIME, Comput. Phys. Commun. 183 (2012) 1321–1335. 1106.4177. https://doi.org/10.1016/j.cpc.2012.01.016

[32] A. Frommer, K. Kahl, S. Krieg, B. Leder, M. Rottmann, Adaptive aggregation-based domain decomposition multigrid for the lattice Wilson–Dirac operator, SIAM J. Sci. Comput. 36 (4) (2014) A1581–A1608. 1303.1377. https://doi.org/10.1137/130919507

[33] C. Alexandrou, S. Bacchio, J. Finkenrath, A. Frommer, K. Kahl, M. Rottmann, Adaptive aggregation-based domain decomposition multigrid for twisted mass fermions, Phys. Rev. D 94 (11) (2016) 114509. 1610.02370. https://doi.org/10.1103/PhysRevD.94.114509

[34] S. Bacchio, C. Alexandrou, J. Finkerath, Multigrid accelerated simulations for twisted mass fermions, EPJ Web Conf. 175 (2018) 02002. 1710.06198. https://doi.org/10.1051/epjconf/201817502002

[35] C. Alexandrou, S. Bacchio, J. Finkenrath, Multigrid approach in shifted linear systems for the non-degenerated twisted mass operator, Comput. Phys. Commun. 236 (2019) 51–64. 1805.09584. https://doi.org/10.1016/j.cpc.2018.10.013

[36] B. Joó, D.D. Kalamkar, T. Kurth, K. Vaidyanathan, A. Walden, Optimizing Wilson-Dirac operator and linear solvers for intel® KNL, in: High Performance Computing: ISC High Performance 2016 International Workshops, ExaComm, E-MuCoCoS, HPC-IODC, IXPUG, IWOPH, P̂ 3MA, VHPC, WOPSSS, Frankfurt, Germany, June 19–23, 2016, Revised Selected Papers 31, Springer, 2016, pp. 415–427.

[37] M. Schröck, S. Simula, A. Strelchenko, Accelerating twisted mass LQCD with QPhiX, PoS LATTICE2015 (2016) 030. 1510.08879. https://doi.org/10.22323/1.251.0030

[38] M.A. Clark, R. Babich, K. Barros, R.C. Brower, C. Rebbi, Solving lattice QCD systems of equations using mixed precision solvers on GPUs, Comput. Phys. Commun. 181 (2010) 1517–1528. 0911.3191. https://doi.org/10.1016/j.cpc.2010.05.002

[39] R. Babich, M.A. Clark, B. Joo, G. Shi, R.C. Brower, S. Gottlieb, Scaling lattice QCD beyond 100 GPUs, in: SC11 International Conference for High Performance Computing, Networking, Storage and Analysis Seattle, Washington, November 12–18, 2011, 2011. 1109.2935. https://doi.org/10.1145/2063384.2063478

[40] M.A. Clark, B. Joó, A. Strelchenko, M. Cheng, A. Gambhir, R.C. Brower, Accelerating lattice QCD multigrid on GPUs using fine-grained parallelization, in: SC '16: Proceedings of the International Conference for High Performance Computing, Networking, Storage and Analysis, 2016, pp. 795–806. 1612.07873. https://doi.org/10.1109/SC.2016.67